AIAA Aviation
16-20 June 2014, Atlanta, GA
32nd AIAA Applied Aerodynamics Conference

2014-2152

Propeller-Induced Flow Effects on Wings of Varying Aspect Ratio at Low Reynolds Numbers

Gavin K. Ananda,* Robert W. Deters,† and Michael S. Selig‡
Department of Aerospace Engineering, University of Illinois at Urbana–Champaign, Urbana, IL 61801, USA

Wind tunnel measurements of rectangular flat-plate wings of varying aspect ratios ($\mathcal{AR}$ = 2, 3, and 4) under different propeller-induced flow conditions were taken at Reynolds numbers from 60,000 to 90,000. The GWS 5×4.3 and GWS 3×3 propellers were used in both the tractor and pusher configurations at various advance ratios. In the tractor configuration, all wings tested showed a reduction in the wing lift curve slope for propellers rotating close to or in the windmill-brake state. As propeller rotation rate increased (decreasing advance ratio), the wing lift curve slope was observed to increase. Negligible variation in lift curve slope was found, however, for the propeller in the pusher configuration. In addition, all wings tested exhibited significant stall delay and increased maximum lift characteristics due to propeller-induced flow effects. The degree of stall delay and maximum lift increase was found to be related to the propeller advance ratio and the propeller diameter-to-wingspan ratio. Most notably, flat-plate wings with an aspect ratio of 2 (high propeller diameter-to-wingspan ratio) with the propeller in both tractor and pusher configurations showed the largest stall delay and maximum lift increase (>40%) at the lowest advance ratios tested. As aspect ratio increased (larger propeller diameter-to-wingspan ratio), the degree of stall delay and maximum lift increase reduced. Also, propellers in the pusher configuration were found to have larger stall delay and maximum lift effects for wings of higher aspect ratio. The results found from these tests underscore the importance of accounting for propeller-wing interaction effects in the design of small-scale UAVs.

Nomenclature

$\mathcal{AR}$	=	aspect ratio
b	=	wingspan
c	=	wing chord
C_L	=	wing lift coefficient ($= L/\frac{1}{2}\rho V_\infty^2 S_{ref}$)
C_D	=	wing drag coefficient ($= D/\frac{1}{2}\rho V_\infty^2 S_{ref}$)
$C_{M_{c/4}}$	=	wing moment coefficient at quarter chord ($= M/\frac{1}{2}\rho V_\infty^2 S_{ref} c$)
C_P	=	propeller power coefficient
C_T	=	propeller thrust coefficient
D	=	propeller diameter, drag
J	=	propeller advance ratio
L	=	lift
LE	=	leading edge
M	=	moment
n	=	propeller rotation rate in rotations per second

*Graduate Student (Ph.D.), 104 S. Wright St., AIAA Student Member. anandak1@illinois.edu
†Graduate Student (Ph.D.), 104 S. Wright St., AIAA Student Member. rdeters@illinois.edu
‡Associate Professor, 104 S. Wright St., AIAA Associate Fellow. m-selig@illinois.edu

Q	=	propeller torque
Re	=	Reynolds number based on wing chord ($= V_\infty c/\nu$)
S_{ref}	=	wing reference area
TE	=	trailing edge
V_∞	=	freestream velocity
α	=	wing angle of attack
η	=	propeller efficiency
λ	=	taper ratio
ν	=	kinematic viscosity
ρ	=	density of air
Ω	=	propeller rotation rate in rotations per minute

Subscripts

$c/4$	=	quarter-chord

I. Introduction

With the rapid growth in the demand of small-scale Unmanned Aerial Vehicles (UAVs) and Micro Air Vehicles (MAVs) both militarily and commercially over the past two decades, there has been a pressing need for more research in this field. Small-scale UAVs operate at Reynolds numbers of up to 300,000 and tend to have low-to-moderate aspect ratio ($2 \leq \mathcal{AR} \leq 7$) wings. At this scale, the propeller diameter-to-wingspan ratio of these UAVs tends to be large. Therefore, given that a substantial portion of the UAV wingspan is affected by the induced flow due to the propeller, there is a necessary need to research the aerodynamic effects of propeller-induced flow on wings at low Reynolds numbers.

A number of steady-state propeller-wing interaction studies have been performed since the 1940s and 50s at Reynolds numbers larger than 350,000.[1–12] As detailed in Ref. 13, a limited amount of literature, however, exists concerning propeller-wing interaction studies at low Reynolds numbers.[13–18] Also, interestingly, results obtained from literature have shown somewhat of a discrepancy regarding the effects of the propeller-induced flow on wing performance. Witkowski et al.[8,9] and previous research by the current authors[13] have observed an increase in lift-to-drag ratio at low angles of attack due to propeller-induced flow in the tractor configuration. However, tests performed by Null et al.[14] showed contradictory effects. A reduction in lift-to-drag ratio was observed at low angles of attack when under similar propeller slipstream conditions. Wings with an aspect ratio of 4 and larger were tested by Refs. 8, 9, and 13. On the other hand, Ref. 14 tested models that had an aspect ratio of 1 leading the current authors to surmise that, apart from variations caused by airfoil differences, the aerodynamic effects of propeller-induced flow conditions on wings at low Reynolds numbers may substantially vary with aspect ratio and propeller location.

As a result, propeller-induced flow wind tunnel experiments have been performed on rectangular flat-plate wings with aspect ratios of 2, 3, and 4 at Reynolds numbers from 60,000 to 90,000. Experiments were performed using a GWS 5×4.3 and GWS 3×3 propeller in both tractor and pusher configurations at various advance ratios (rotation rates).

II. Experimental Methods

A. Facility

All experiments were conducted at the low turbulence subsonic wind tunnel located at the Aerodynamic Research Lab at the University of Illinois at Urbana-Champaign (UIUC). The wind tunnel is an open-return tunnel with a rectangular test section that measures 2.8 × 4.0 ft (0.853 × 1.219 m) in cross-section and 8 ft (2.438 m) in length. Over the length of the test section, the width of the tunnel cross section increases by approximately 0.5 in (12.7 mm) to account for boundary layer growth along the tunnel side walls. Test

section speeds of up to 160 mph (71.53 m/s) can be obtained via a 125 hp (93.25 kW) alternating current electric motor connected to a five-bladed fan. As detailed in Ref. 19, the turbulence intensity of the wind tunnel was measured to be less than 0.1%.

B. Experimental Setup

The experimental setup consisted of a three-component low Reynolds number force balance (LRN-FB) and a propeller fairing setup as depicted in Figs. 1 and 2. The LRN-FB measured the aerodynamic loads of the wing under different propeller-induced flow conditions. The propeller fairing setup provided the wing with the specific propeller-induced flow conditions. The experimental setup was created in such a way that the propeller fairing setup and the LRN-FB were not physically attached to one another. In this way, it was possible to isolate the effect of the induced flow due to the propeller on wing measurements with the LRN-FB.

The LRN-FB was a custom designed and in-house fabricated external three-component platform force balance. The design, assembly, and validation of the LRN-FB are described in detail in Refs. 20 and 21. Additional details of the propeller fairing setup can be found in Ref. 13.

C. Data Acquisition

A PC with a National Instruments NI PCI-6052E data acquisition board (DAQ) was used for communication with the wind tunnel, LRN-FB, and propeller fairing setup. Test section dynamic pressure was measured with a differential pressure transducer in the wind tunnel inlet and test section. Ambient temperature was measured with a thermocouple. Lift, drag, and moment data from the load cells in the LRN-FB were passed through a signal conditioner to amplify and filter the signals for the DAQ board. At each angle of attack, 30,000 contiguous samples of lift, drag, and moment were measured at a rate of 3,000 samples/s and averaged to overcome the small time-dependent fluctuations in the measurements. Each run involved taking

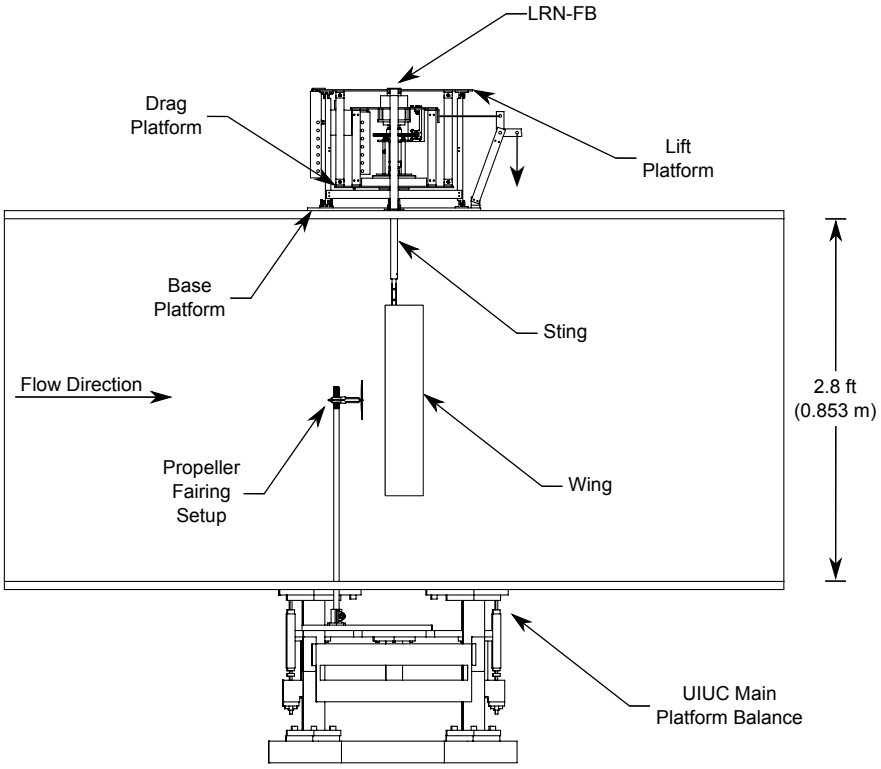

Figure 1. UIUC LRN-FB and propeller fairing setup in the tunnel test section (tractor configuration).

2014-2152

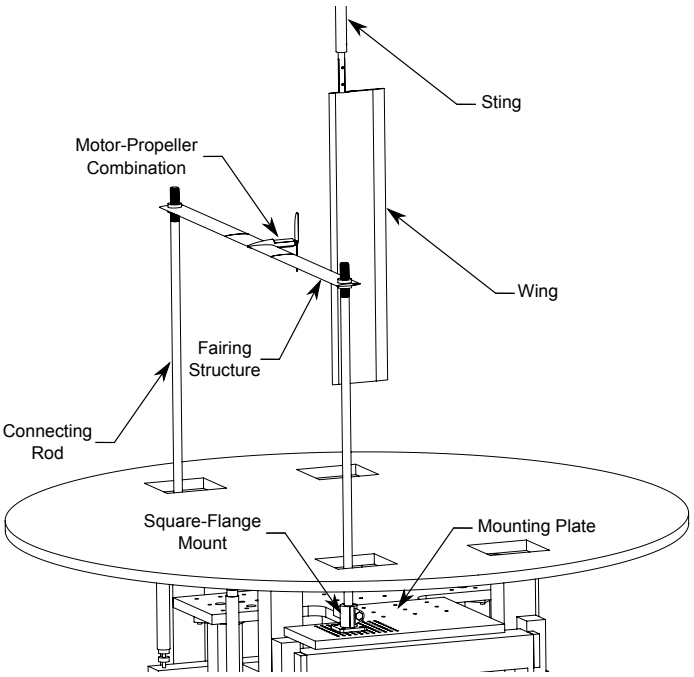

Figure 2. Isometric view of the propeller fairing setup in tunnel test section (tractor configuration).

measurements of the wing for both increasing and decreasing angles of attack in succession to capture any possible aerodynamic hysteresis.

During a run, the entire data-acquisition process was automated. The LabVIEW® interface set and maintained the Reynolds number of the wind tunnel, the RPM of the motor, the angle of attack of the wing, the angle of attack of the propeller, acquired raw data, and finally reduced and plotted the data graphically during a run for realtime inspection. Once the run was complete, the data was corrected for three-dimensional tunnel effects according to the methods outlined in Ref. 22. The relative uncertainties of the lift, drag, and moment coefficients were calculated to be 3.3%, 2.7%, and 4.6%, respectively, using the methods introduced by Kline and McClintock [23] and further discussed by Coleman and Steel. [24]

D. Models Tested

Three rectangular wings with aspect ratios of 2, 3, and 4 were tested. The wings used a 4.3% thick flat-plate airfoil that had a 5-to-1 elliptical leading edge and a 10-to-1 elliptical trailing edge. The wings were rapid prototyped using SLA® to tolerances of approximately ±0.005 in, ensuring model accuracy and surface quality. All wings had a chord length (c) of 3.5 in (88.9 mm). Performance data and design information for the flat-plate wings can be found in Refs. 20 and 21.

The GWS 5×4.3 propeller had a diameter of 5 in (127 mm) and a pitch of 4.3 in (109.2 mm) and the GWS 3×3 propeller had a diameter of 3.2 in (81.3 mm) and pitch of 3 in (76.2 mm). The propellers were chosen as there were performance data available, and the diameters were appropriate given the 3.5 in chord length of the flat-plate wings. Performance data for the GWS propellers can be found in Section III.

Table 1 lists the experimental test matrix. The three wings were tested in the tractor and pusher configurations with both propellers under varying advance ratios (rotation rates). Tests were performed at Reynolds numbers of 60,000, 70,000, 80,000, and 90,000. A total of 94 propeller-induced flow effect data sets were taken in addition to the clean wing and fairing only (no propeller) results taken for each configuration and Reynolds number tested. The location of the propellers were set based on the 1/2-diameter location from the wing leading edge (LE) for the propeller in the tractor configuration and the 1/4-diameter location from the wing trailing edge (TE) for the propeller in the pusher configuration and was accurate to ±0.1 in (2.5 mm).

Table 1. Experimental Test Matrix

Aspect Ratio	Propeller	Configuration	Re	Ω	J
2,3,4	GWS 5×4.3	Tractor (2.5 in from LE)	60,000	6,000 RPM	0.80
				7,000 RPM	0.69
				8,000 RPM	0.60
			70,000	7,000 RPM	0.81
				8,000 RPM	0.70
				9,000 RPM	0.64
			80,000	7,000 RPM	0.92
				8,000 RPM	0.81
				9,000 RPM	0.72
			90,000	9,000 RPM	0.81
		Pusher (1.25 in from TE)	60,000	6,000 RPM	0.82
				7,000 RPM	0.70
				8,000 RPM	0.61
			70,000	7,000 RPM	0.81
				8,000 RPM	0.71
				9,000 RPM	0.63
			80,000	7,000 RPM	0.93
				8,000 RPM	0.81
				9,000 RPM	0.71
			90,000	9,000 RPM	0.81
	GWS 3×3	Tractor (1.6 in from LE)	60,000	7,000 RPM	1.09
				9,500 RPM	0.81
				12,000 RPM	0.64
			70,000	12,000 RPM	0.73
			80,000	12,000 RPM	0.83
			90,000	12,000 RPM	0.94
		Pusher (0.8 in from TE)	60,000	7,000 RPM	1.08
				9,500 RPM	0.80
				12,000 RPM	0.63
			70,000	12,000 RPM	0.74
			80,000	12,000 RPM	0.84
			90,000	12,000 RPM	0.95

All tests were performed with the propeller centerline aligned with the chordline of the wing to an accuracy of ±0.08 in (2 mm). The locations of the GWS 5×4.3 propeller in the tractor and pusher configurations with respect to a flat-plate wing are shown in Fig. 3.

III. Performance Data for the GWS 5×4.3 and GWS 3×3 Propellers

Results from the static performance tests for the GWS 5×4.3 and GWS 3×3 propellers are shown in Figs. 4(a) and 4(b), respectively. In addition, advancing-flow performance results are shown in Figs. 5 and 6 for the two respective propellers. Note that the Reynolds number displayed in Figs. 4–6 is for the propeller and is defined by the chord and rotational speed at the 75% blade station.

Performance data for the GWS 5×4.3 and GWS 3×3 propellers were gathered using a wind tunnel testing rig designed to measure propeller thrust and power. More information on the setup and procedure to test these propellers can be found in Deters et al.[25,26] and Brandt.[27] An Interface SMT S-Type load cell with a load capacity of 2.2 lb (9.8 N) measured thrust, and a Transducer Techniques RTS-5 5 oz-in (0.0353 N-m) torque cell was used to measure torque. From the torque measurements, the power was calculated by

$$P = 2\pi n Q \tag{1}$$

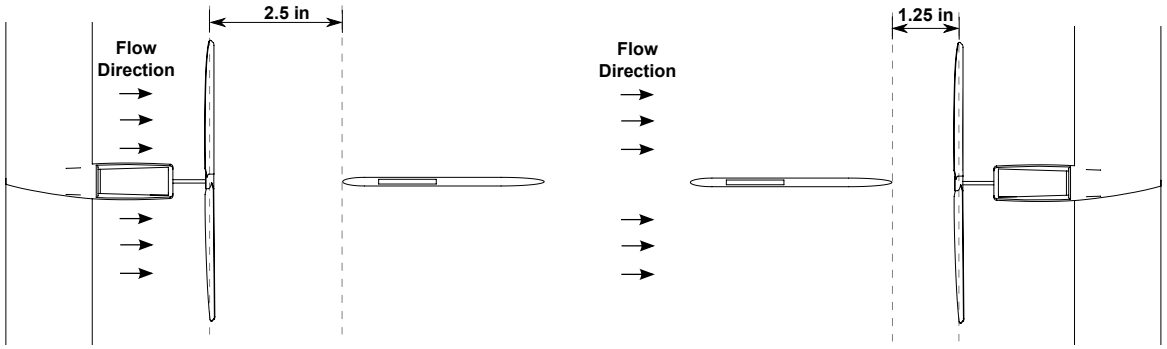

Figure 3. Top view of flat-plate wing with GWS 5×4.3 propeller in the (a) tractor and (b) pusher configuration.

where n is the rotational speed measured in rotations per second and Q is the torque. Thrust and power coefficients (C_T and C_P) were calculated using the rotational speed and diameter, respectively, with the following equations

$$C_T = \frac{T}{\rho n^2 D^4} \tag{2}$$

$$C_P = \frac{P}{\rho n^3 D^5} \tag{3}$$

For static conditions, the propellers were tested over a range of rotational speeds, and for tests with a freestream velocity, the propellers were tested over a range of advance ratios (J) calculated by

$$J = \frac{V}{nD} \tag{4}$$

During advancing-flow tests (wind tunnel on), the propeller was set to run at a constant rotational speed, and the flow speed was increased from 8 ft/s to a flow speed near the onset of windmilling. The efficiency of

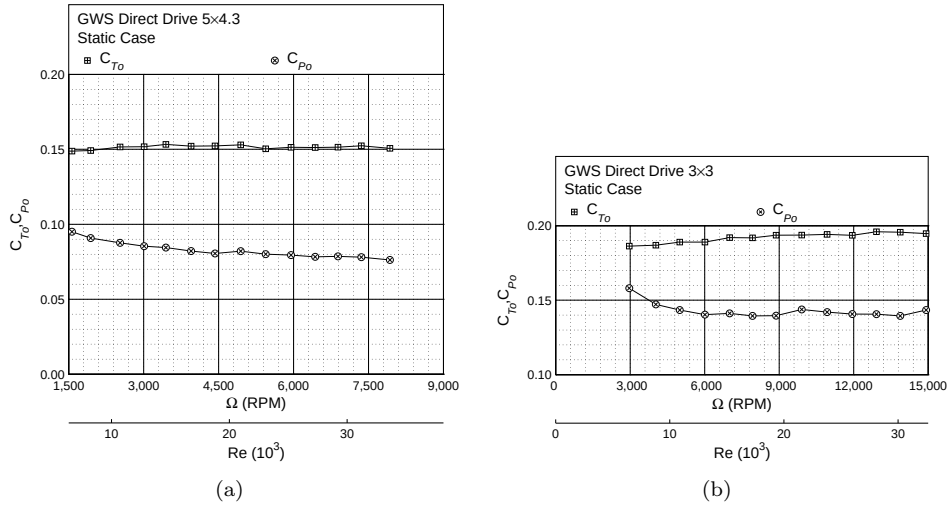

Figure 4. Static performance data for the (a) GWS 5×4.3 and (b) GWS 3×3 propellers.

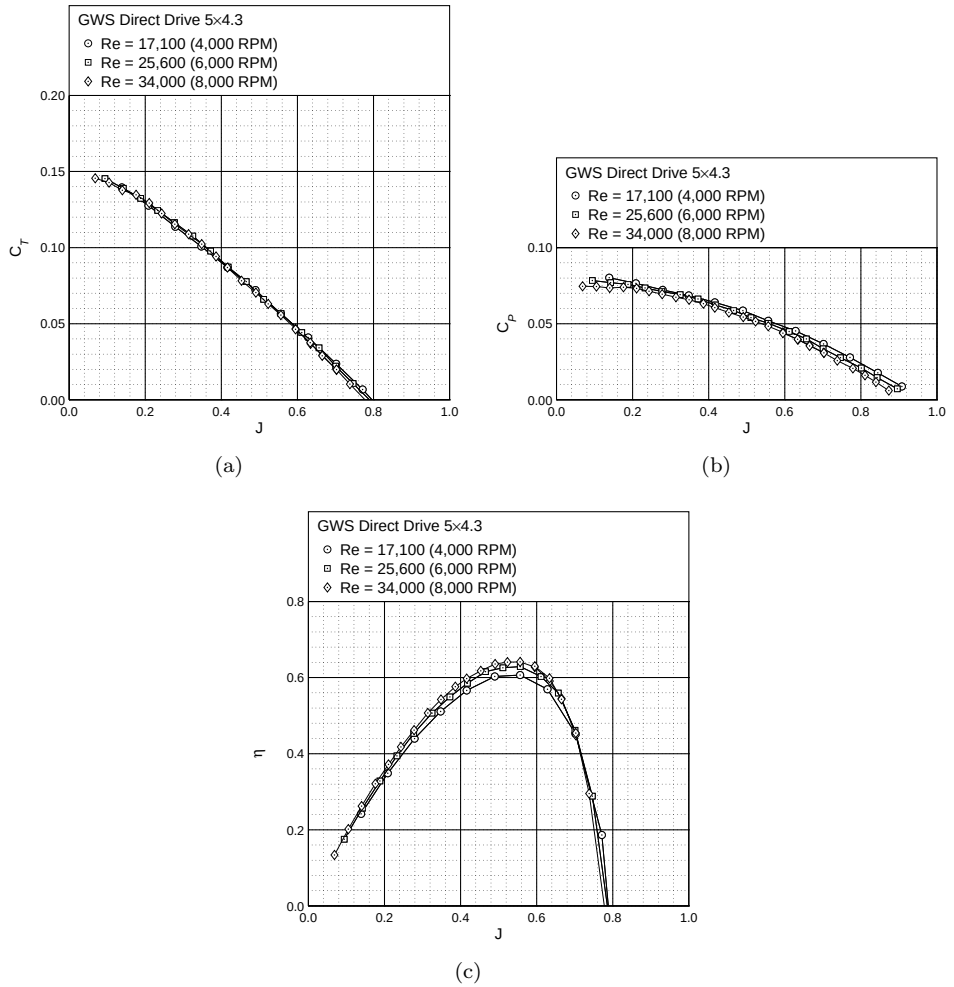

Figure 5. GWS 5×4.3 performance data: (a) thrust coefficient, (b) power coefficient, and (c) efficiency curve.

the propeller during these tests was also calculated by

$$\eta = \frac{C_T J}{C_P} \tag{5}$$

The windmill-brake state ($C_T < 0$) for the GWS 5×4.3 and GWS 3×3 propellers were found from the C_T performance data [Figs. 5(a) and 6(a)] to occur at advance ratios of $J = 0.8$ and $J = 0.97$, respectively. From Table. 1, it can be seen that multiple propeller-induced flow test cases were performed with either propeller (GWS 5×4.3 or GWS 3×3), in or close to the windmill-brake state. Note that in the windmill-brake state, the flow behind the propeller is being reduced (i.e. propeller is creating drag and not thrust).

IV. Results and Discussion

Wind tunnel measurements are presented in this section for the experimental test parameters outlined in Table 1. Most measurements were taken from −15 to 25 deg at both increasing and decreasing angles of attack. Lift, drag, and moment results for the rectangular flat-plate wings are presented in this paper. The discussion of the results are presented in terms of the different effects tested (varying advance ratio and aspect ratio) where comparisons are made in terms of the propeller location (tractor or pusher) with respect to the wing.

Given that propeller-induced flow wind tunnel measurements necessitated the use of a propeller fairing

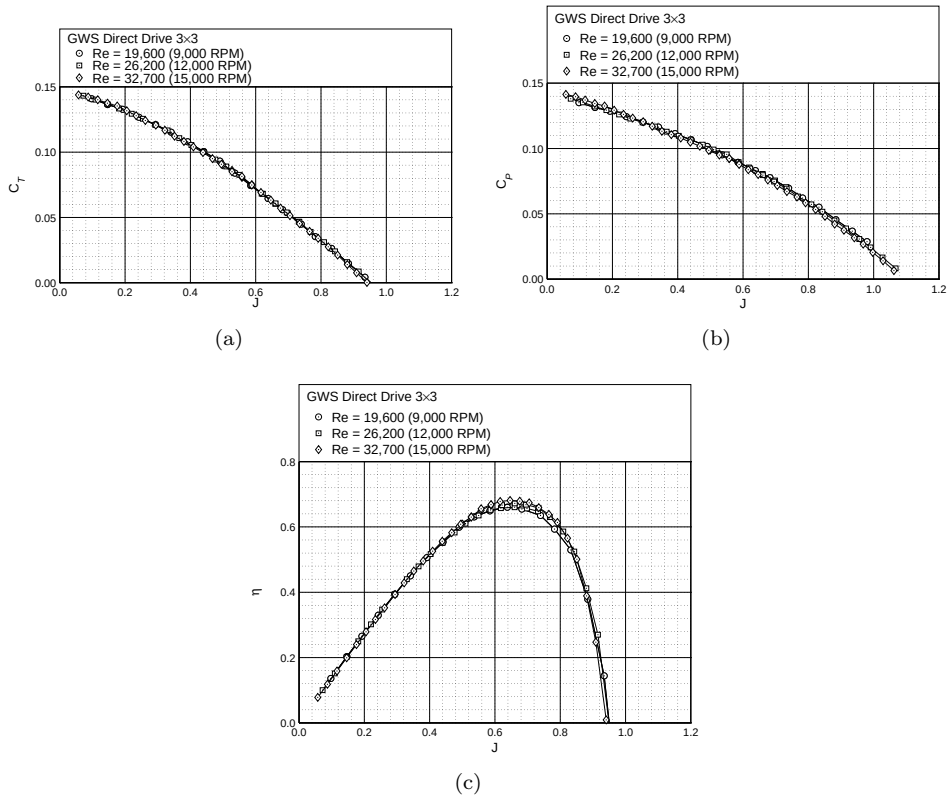

Figure 6. GWS 3×3 performance data: (a) thrust coefficient, (b) power coefficient, and (c) efficiency curve.

(discussed in Section II), it was imperative that the effect of the propeller fairing itself was accounted for in the discussions of the results presented. Therefore, in most of the proceeding figures, 'Fairing Only' results will also be included to supplement the other results presented. Note that 'Fairing Only' results mean that no propeller was attached to the motor during these tests.

A. Effect of Advance Ratio

The effect of varying propeller advance ratio (rotation rate) on the aerodynamic performance of flat-plate wings with aspect ratios of 2, 3, and 4 were tested at different Reynolds numbers. Representative lift, drag, and moment results for an aspect ratio 4 flat-plate wing at a Reynolds number of 80,000 are presented in terms of the different configurations tested (tractor or pusher) in the proceeding subsections.

1. Lift

Clean, fairing only, and varying GWS 5×4.3 propeller advance ratio (rotation rate) lift results for the aspect ratio 4 wing are shown in both the tractor and pusher configurations in Fig. 7. From Fig. 7(a) (tractor configuration), a variation in the lift curve slope is observed at pre-stall angles of attack from the clean wing test case due to varying propeller advance ratio (rotation rate). Changes in the lift curve slope are, however, not evident for the pusher configuration case [Fig. 7(b)].

To more clearly illustrate the lift curve slope variations observed, calculated lift curve slopes for the aspect ratio 4 flat-plate wing are presented as a function of Reynolds number for the two configurations and propellers (GWS 5×4.3 and GWS 3×3) tested in Figs. 8 and 9. As per Table 1, a total of 18 lift curve slopes (10 propeller-induced flow test cases) were used to populate Figs. 8(a) and 8(b). A total of 14 lift curve slopes (6 propeller-induced flow test cases) were used to populate Figs. 9(a) and 9(b). In the tractor configuration, fairing only measurements for both propellers show a 0.5–3% increase in lift curve slope from

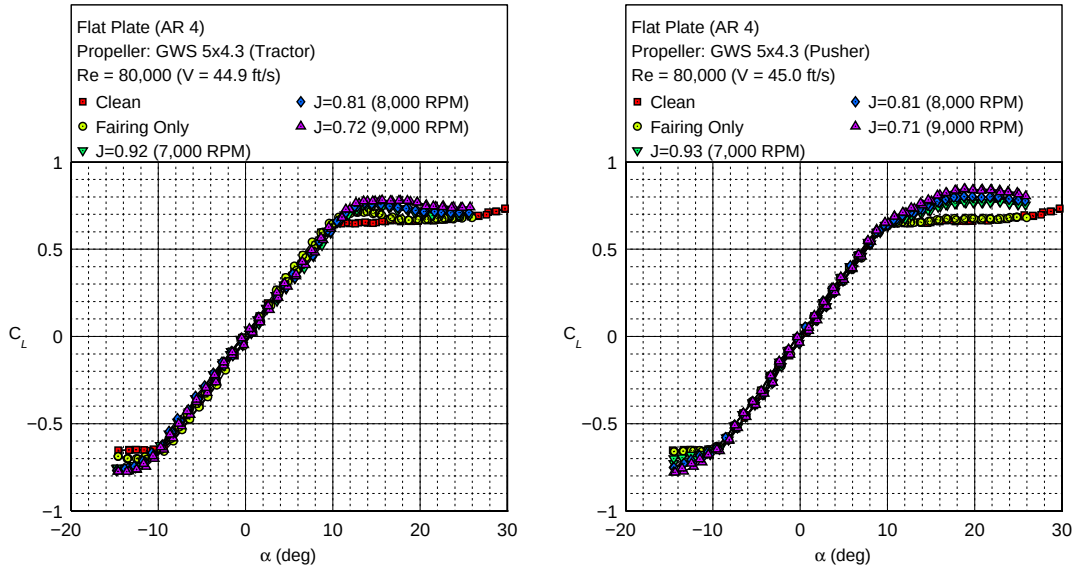

(a) (b)

Figure 7. Effect of increasing propeller rotation rate (Ω) on the lift curve of the flat-plate *AR*-4 rectangular wing at a Reynolds number of 60,000 in the (a) tractor and (b) pusher configuration.

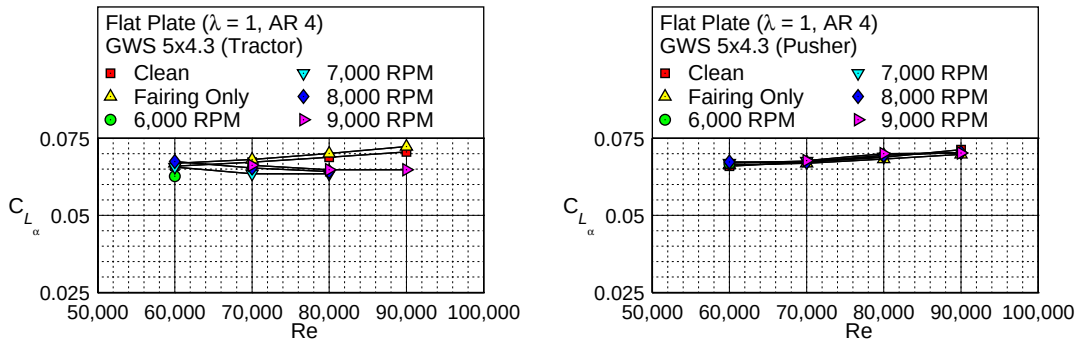

(a) (b)

Figure 8. Effect of Reynolds number on the lift curve slope, C_{L_α}, for the flat-plate *AR*-4 rectangular wing and the GWS 5×4.3 propeller in the (a) tractor and (b) pusher configuration.

the clean wing case at the Reynolds numbers tested. On the other hand, negligible variation is observed in the lift curve slopes between the clean and fairing only cases for the pusher configuration tests.

For the tractor configuration tests [Figs. 8(a) and 9(a)], a reduction in lift curve slope is observed for a number of test cases. The lift curve slope reductions seem to be related to the propeller advance ratio. Test cases with advance ratios close to or in the windmill-brake state (see Section III) exhibit reductions in C_{L_α} from the clean wing case. From Table 1, a number of GWS 5×4.3 test cases occur close to the propeller windmill-brake state ($J = 0.8$). As a result, Fig. 8(a) shows non-negligible reductions in the lift curve slope. At a Reynolds number of 60,000, a lift curve slope drop of ∼0.003 per deg (5% decrease) is observed in Fig. 8(a) for a propeller rotation rate of 6,000 RPM ($J = 0.8$). At a Reynolds number of 90,000, an 8.3% reduction in the lift curve slope is observed for a propeller rotation rate of 9,000 RPM ($J = 0.81$). It is important to note that as the propeller rotation rate increases (decreasing advance ratio), the lift curve slope of the wing increases at all Reynolds numbers tested. The relationship between the propeller in the windmill-

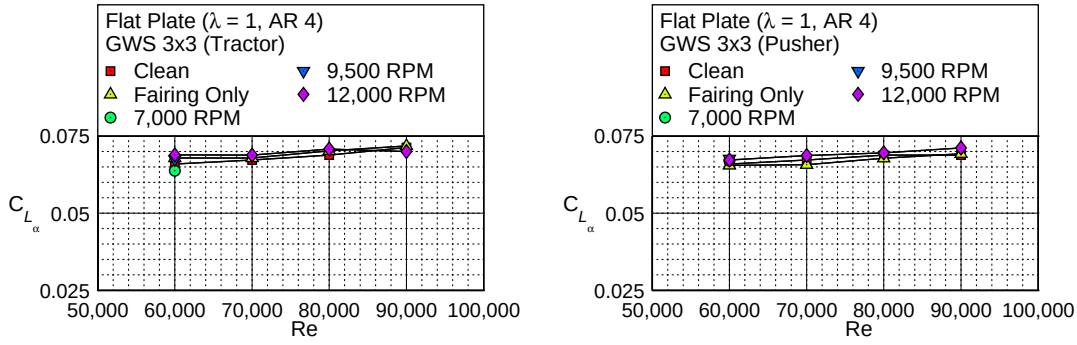

(a) (b)

Figure 9. Effect of Reynolds number on the lift curve slope, C_{L_α}, for the flat-plate $\mathcal{AR}$-4 rectangular wing and the GWS 3×3 propeller in the (a) tractor and (b) pusher configuration.

brake state and its effect on lift curve slope reduction is reinforced in Fig. 9(a) where from Table 1, the only two test cases operating at advance ratios close to the GWS 3×3 propeller windmill-brake state ($J = 0.97$) are the Re = 60,000, Ω = 7,000 RPM ($J = 1.09$) and the Re = 90,0000, Ω = 12,000 RPM ($J = 0.94$) test cases. Both these test cases were the only lift curves slopes that showed reductions (3.3% and 1.8% respectively) from the clean wing case. Pusher configuration results for both propellers [Fig. 8(b) and 9(b)] exhibited a slight increase or negligible variation in lift curve slope with increasing propeller rotation rate from the clean wing case for both propellers.

Another important observation from the lift curves in Fig. 7 is the stall delay and increasing maximum lift effects due to decreasing advance ratio (increasing rotation rate). The propeller-induced flow for both configurations causes the $C_{L_{max}}$ and α_{stall} to significantly increase with increasing propeller rotation rate (decreasing advance ratio). The $C_{L_{max}}$ values as a function of Reynolds number for the aspect ratio 4 wing are presented in Figs. 10 and 11 for the two configurations (pusher/tractor) and propellers (GWS 5×4.3/GWS 3×3) tested. The propeller fairing causes an average $C_{L_{max}}$ decrease of 3.4% and 6.3% from the clean wing case for the tractor and pusher configurations, respectively. For the GWS 5×4.3 propeller in the tractor configuration [Fig. 10(a)], a maximum $C_{L_{max}}$ increase of 3.5% (Re =90,000, Ω = 9,000 RPM, $J = 0.81$) to 19.7% (Re =60,000, Ω = 8,000 RPM, $J = 0.6$) is observed. For the GWS 5×4.3 propeller in the pusher configuration [Fig. 10(b)], a $C_{L_{max}}$ increase of 7.8% (Re =90,000, Ω = 9,000 RPM, $J = 0.81$) to 30.2% (Re =60,000, Ω = 8,000 RPM, $J = 0.61$) is observed. The stall delay and $C_{L_{max}}$ increasing effect is

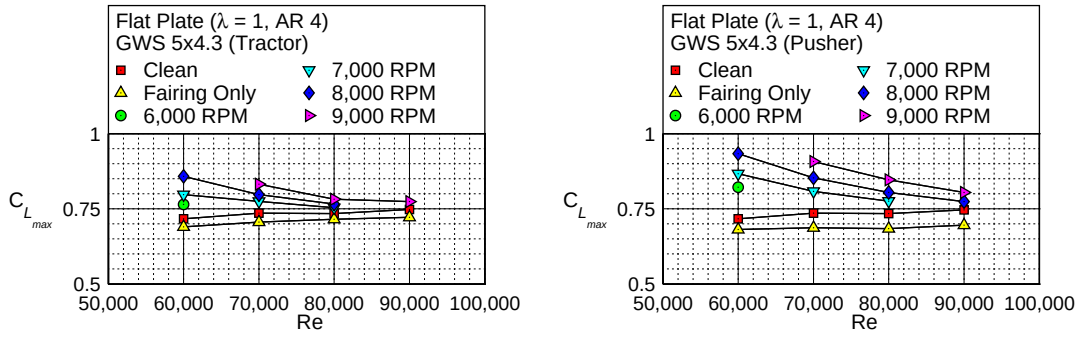

(a) (b)

Figure 10. Effect of Reynolds number on the maximum lift, $C_{L_{max}}$, for the rectangular flat plate wing with an aspect ratio of 4 and GWS 5×4.3 propeller in the (a) tractor and (b) pusher configuration.

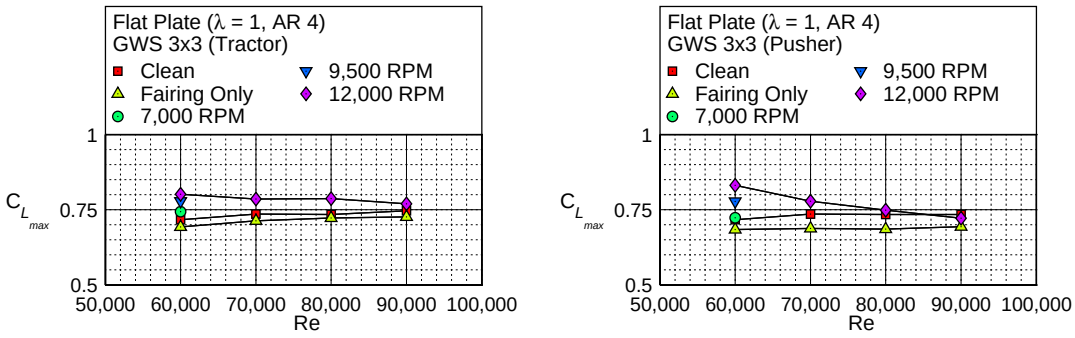

(a) (b)

Figure 11. Effect of Reynolds number on the maximum lift, $C_{L_{max}}$, for the flat-plate $\mathcal{AR}$-4 rectangular wing and the GWS 3×3 propeller in the (a) tractor and (b) pusher configuration.

related to the decreasing advance ratio of each propeller and is more pronounced for propellers in the pusher configuration. In addition, comparing Figs. 10 and 11, there seems to be an added importance related to the propeller diameter-to-wingspan ratio (D/b), where, a lower D/b ratio is observed to reduce the effect of the propeller-induced flow in delaying stall and increasing maximum lift.

2. Drag

Clean, fairing only, and varying GWS 5×4.3 propeller advance ratio (rotation rate) drag results for the aspect ratio 4 wing are shown in both the tractor and pusher configurations at a Reynolds number of 80,000 in Fig. 12. To more easily show the differences between the drag curves in Fig. 12, results are presented in terms of the change in drag (ΔC_D) from the clean wing configuration in Fig. 13. Tractor and pusher configuration results for the aspect ratio 4 wing at low angles of attack (< 6 deg) show that the drag

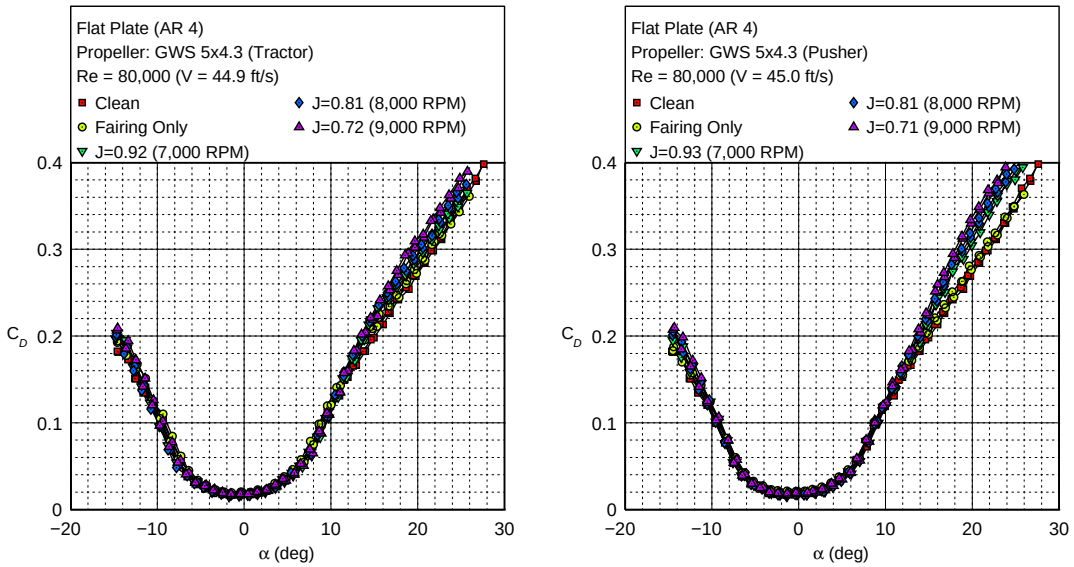

(a) (b)

Figure 12. Effect of increasing propeller rotation rate (Ω) on the drag curve of the flat-plate $\mathcal{AR}$-4 rectangular wing at a Reynolds number of 60,000 in the (a) tractor and (b) pusher configuration.

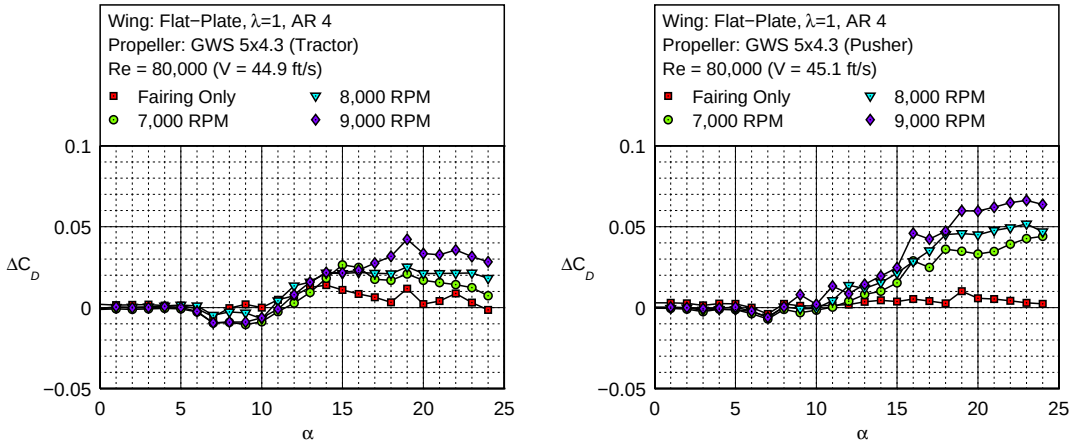

(a) (b)

Figure 13. Change in C_D from the clean wing case for the flat-plate $\mathcal{AR}$-4 rectangular wing at a Reynolds number of 80,000 and the GWS 5×4.3 propeller in the (a) tractor and (b) pusher configuration.

coefficient is negligibly affected by variation in propeller rotation rate from the clean wing case. At high angles of attack ($\geq$ 11 deg), though, it is observed that there is an increase in drag with increasing propeller rotation rate for both tractor and pusher configurations. The differences observed between the tractor and pusher configurations is that from 6 to 11 deg a decrease in drag is observed for the tractor configurations results [Fig. 13(a)] in comparison with a limited change in drag observed for the pusher configurations results [Fig. 13(b)].

3. Moment

Clean, fairing only, and varying GWS 5×4.3 propeller advance ratio (rotation rate) moment results for the aspect ratio 4 wing are shown in both the tractor and pusher configurations at a Reynolds number of 80,000 in Fig. 14. Similar to the drag results, the change in moment ($\Delta C_{M_{c/4}}$) is presented in Fig. 15.

The moment coefficient results show negligible variation in the pre-stall moment curve slopes with increasing propeller rotation rate for both configurations. For the tractor configuration results, an increase in

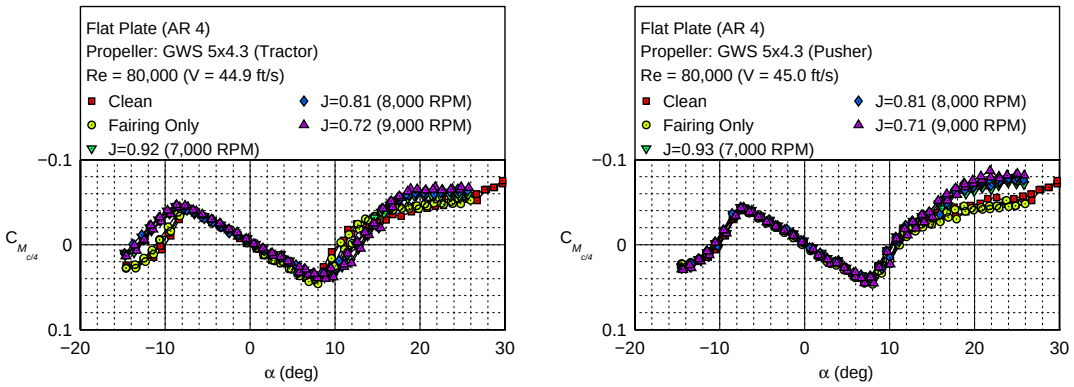

(a) (b)

Figure 14. Effect of increasing propeller rotation rate (Ω) on the moment curve of the flat-plate $\mathcal{AR}$-4 rectangular wing at a Reynolds number of 60,000 in the (a) tractor and (b) pusher configuration.

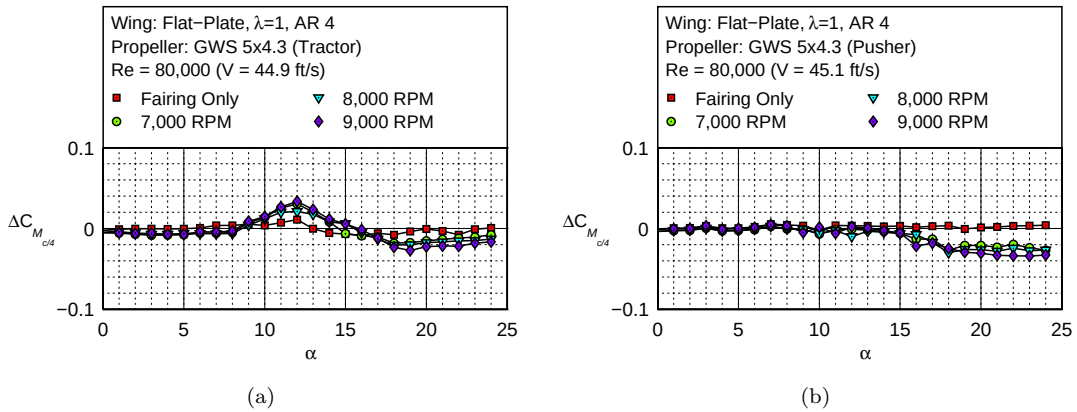

Figure 15. Change in $C_{M_{c/4}}$ from clean wing case for the flat-plate $\mathcal{A}$R-4 rectangular wing at a Reynolds number of 80,000 and the GWS 5×4.3 propeller in the (a) tractor and (b) pusher configuration.

$\Delta C_{M_{c/4}}$ is observed between 9 and 15 deg angle of attack [Fig. 15(a)]. The increase in moment signifies a delay in moment stall with decreasing advance ratio (increasing rotation rate) as shown in Fig. 14(a). At high angles of attack ($\geq$ 15 deg), larger post-stall moments (more negative) are observed in comparison with the clean wing for both tractor and pusher configurations.

B. Effect of Aspect Ratio

In this subsection, aerodynamic performance results showing the effect of aspect ratio variation under propeller-induced flow conditions are presented at Reynolds numbers of 60,000 and 80,000.

1. Lift

The effect of aspect ratio variation on the lift curve is shown in Fig. 16. Flat-plate wing results for both a clean wing and a GWS 5×4.3 propeller operating at 8,000 RPM are coplotted for all wings tested at a Reynolds number of 60,000 ($J = 0.60$). The change in lift from the clean wing case (ΔC_L) for the different aspect ratio wings tested is also presented in Fig. 17 for the tractor and pusher configurations.

A $\Delta C_{L_{max}}$ increase as large as 0.35 is observed for both configurations in Figs. 16 and 17 for the aspect ratio 2 wing. The propeller-induced flow $C_{L_{max}}$ values are also observed to occur at a lower angle of attack for the tractor configuration in comparison with the pusher configuration. However, for the pusher configuration, the separation delay effect does not seem to have plateaued at the highest angle of attack tested (25 deg), whereas, the angle of attack plateaus at approximately 23 deg for the tractor configuration. A lower $\Delta C_{L_{max}}$ variation of ∼0.25 is observed for the aspect ratio 3 case, and for the aspect ratio of 4 case, the difference drops to ∼0.2. More notable though, is that as aspect ratio increases, the pusher configuration results are observed to have larger $C_{L_{max}}$ values, as is most clearly shown in the aspect ratio 4 lift curves [Fig. 16(a) and 16(b)].

In Fig. 17, it can be observed that the angle of attack where ΔC_L starts to increase is dependent on the aspect ratio. The ΔC_L increase starts at a lower angle of attack for larger aspect ratio wings (∼9 deg for $\mathcal{A}$R-4, ∼10 deg for $\mathcal{A}$R-3, and ∼13 deg for $\mathcal{A}$R-2) for both the tractor and pusher configurations. In addition, the slope of the increase in ΔC_L for the different aspect ratios tested is similar to each other. When comparing the slope of the two configurations, though, a lower ΔC_L slope is observed for the pusher configuration case owing to its larger stall delay effects. Results for α_{stall} can be extracted from Figs. 16 and 17 and they are as tabulated in Table 2. The results in Table 2 show that wings with propellers in the pusher configuration tend to have larger stall delays in comparison with wings with propellers in the tractor configuration. For both configurations, the stall angle increases as aspect ratio decreases.

The calculated lift curve slope values as a function of aspect ratio for all wings tested are presented in Figs. 18 and 19 for the GWS 5×4.3 and GWS 3×3 propellers, respectively. Results are presented at a

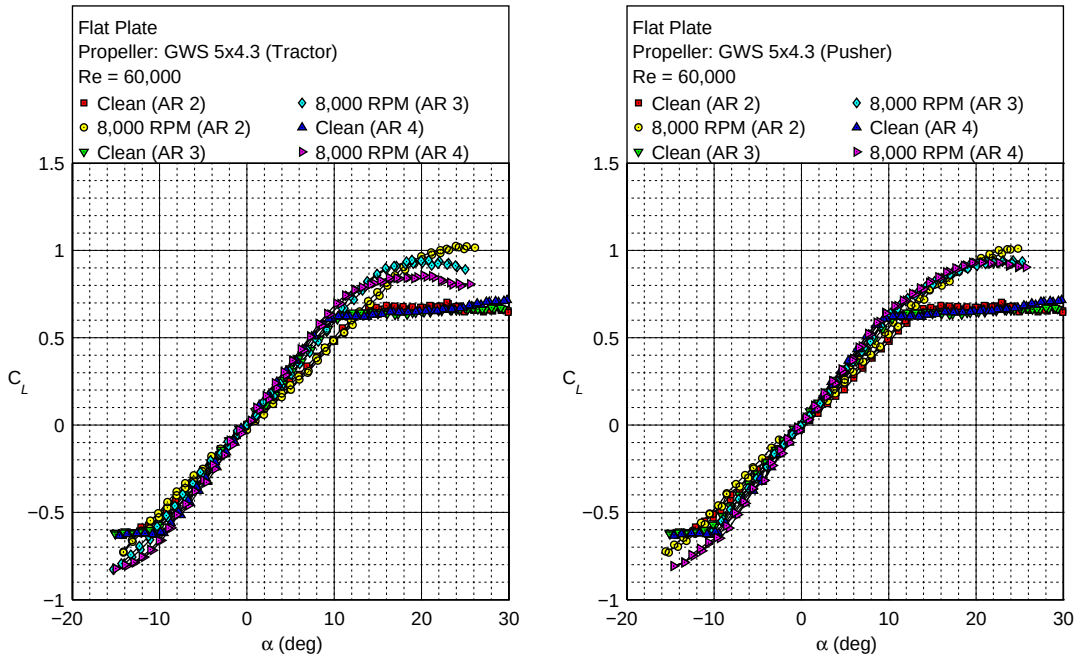

Figure 16. Lift curve comparison of different aspect ratio wings at a Reynolds number of 60,000 and the GWS 5×4.3 propeller at 8,000 RPM ($J = 0.60$) in the (a) tractor and (b) pusher configuration.

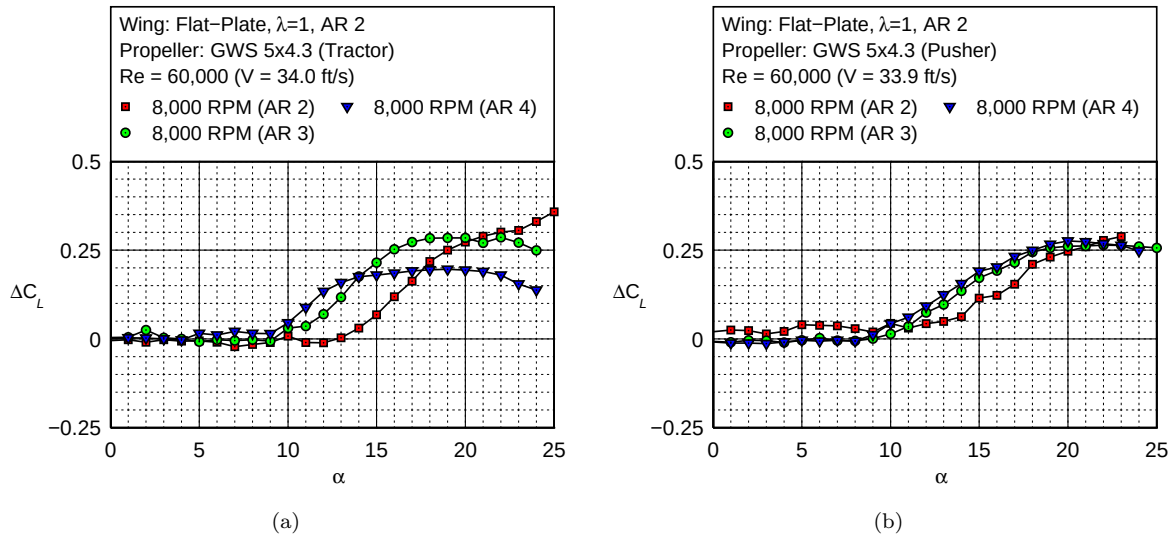

Figure 17. Change in C_L from clean wing case of different aspect ratio wings at a Reynolds number of 60,000 and the GWS 5×4.3 propeller at 8,000 RPM ($J = 0.60$) in the (a) tractor and (b) pusher configuration.

Reynolds number of 60,000 with both propellers in the tractor and pusher configurations. For the GWS 5×4.3 propeller in the tractor configuration, lift curve slopes for the 6,000 RPM ($J = 0.80$), 7,000 RPM ($J = 0.69$), and 8,000 RPM ($J = 0.60$) test cases for each aspect ratio wing are used [Fig. 18(a)]. Similarly, in the pusher configuration, lift curve slopes for the for the 6,000 RPM ($J = 0.82$), 7,000 RPM ($J = 0.70$), and 8,000 RPM ($J = 0.61$) test cases are used [Fig. 18(b)]. For the GWS 3×3 propeller, tractor configuration

Table 2. Approximate α_{stall} values derived from Figs. 16 and 17

Aspect Ratio	α_{stall} (deg) Tractor	Pusher
2	~23	>25
3	~19	~20
4	~17	~18

lift curve slopes for the 7,000 RPM ($J = 1.09$), 9,500 RPM ($J = 0.81$), and 12,000 RPM ($J = 0.64$) test cases are used [Fig. 19(a)], and for the pusher configuration lift curve slopes for the 7,000 RPM ($J = 1.08$), 9,500 RPM ($J = 0.80$), and 12,000 RPM ($J = 0.63$) test cases are used [Fig. 19(b)]. The theoretical lift curve slope for a finite wing of elliptical wing loading (ideal wing) and the Helmbold low aspect ratio straight-wing equation slopes are also co-plotted as lines in Figs. 18 and 19. The ideal theoretical lift curve slope is given by

$$C_{L_\alpha} = C_{l_\alpha} \frac{\mathcal{AR}}{\mathcal{AR} + 2} \tag{6}$$

and the Helmbold equation, taken from Ref. 28, is given by

$$C_{L_\alpha} = C_{l_\alpha} \frac{\mathcal{AR}}{\left(\frac{C_{l_\alpha}}{\pi}\right) + \sqrt{\left(\frac{C_{l_\alpha}}{\pi}\right)^2 + \mathcal{AR}^2}} \tag{7}$$

where C_{l_α} refers to the airfoil lift curve slope taken as 2π.

As discussed in the prior secton, variation is observed in the lift curve slopes of wings in the tractor configuration. A reduction in C_{L_α} from the clean wing case due to the propeller operating close to or in the windmill-brake state is observed for all aspect ratio wings tested as shown in Figs. 18(a) [6,000 RPM ($J = 0.8$) results] and 19(a) [7,000 RPM ($J = 1.09$) results]. The results in Figs. 18(a) and 19(a) and the discussions in the previous section show that the primary factor that determines wing lift curve slope reduction is the propeller advance ratio. There is, however, also a secondary effect exhibited in the results of Figs. 18(a) and 19(a) related to the propeller diameter-to-wingspan ratio (D/b). From Fig. 18(a), for the 6,000 RPM ($J = 0.8$) results, lift curve slope reductions of 13.4%, 7.3%, and 5% are calculated for wings with aspect ratios of 2 ($D/b = 0.71$), 3 ($D/b = 0.48$), and 4 ($D/b = 0.36$), respectively. For a constant

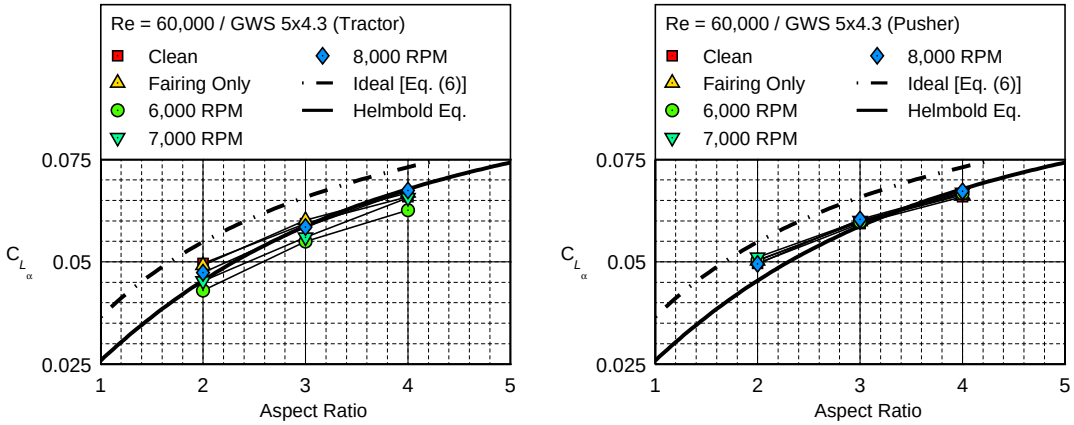

Figure 18. Effect of aspect ratio on the lift curve slope, C_{L_α}, for rectangular flat-plate wings at a Reynolds number of 60,000 with the GWS 5×4.3 propeller in the (a) tractor and (b) pusher configuration.

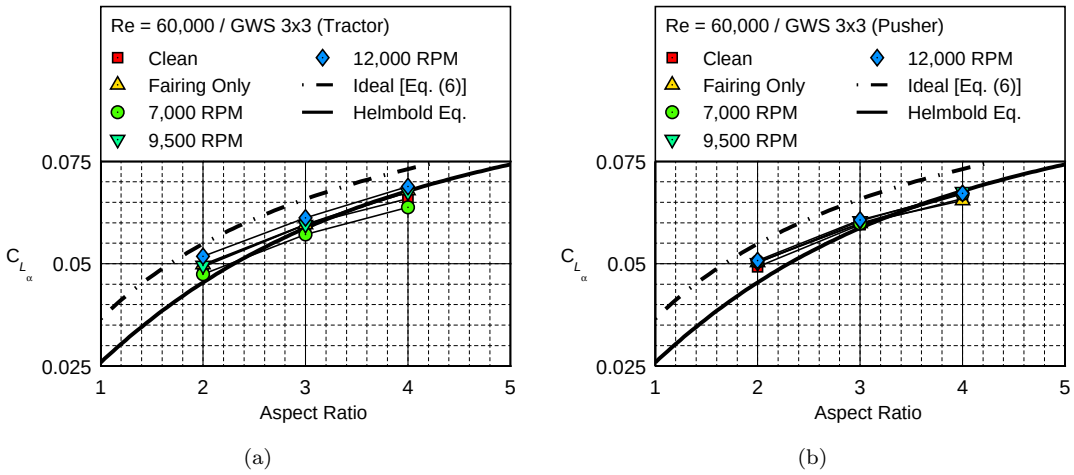

Figure 19. Effect of aspect ratio on the lift curve slope, C_{L_α}, for rectangular flat-plate wings at a Reynolds number of 60,000 with the GWS 3×3 propeller in the (a) tractor and (b) pusher configuration.

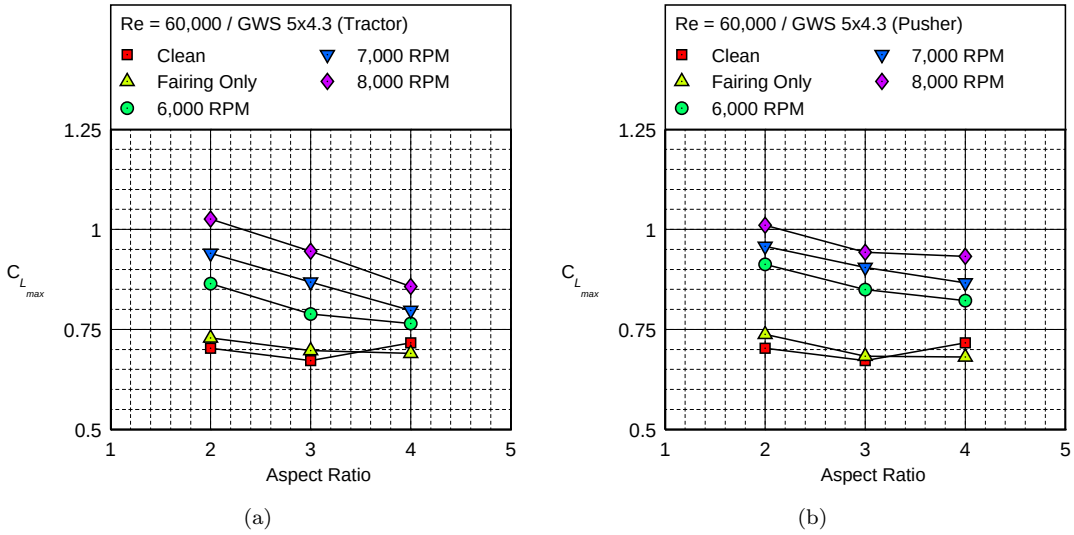

Figure 20. Effect of aspect ratio on the maximum lift, $C_{L_{max}}$, for rectangular flat-plate wings at a Reynolds number of 60,000 with the GWS 5×4.3 propeller in the (a) tractor and (b) pusher configuration.

propeller advance ratio, as propeller diameter-to-wingspan ratio increases (decreasing aspect ratio), the lift curve slope reduction increases owing to the fact that a larger proportion of the wing is within the propeller slipstream. The propeller diameter-to-wing ratio trends found may not always hold true, however, as results from Fig. 19(a) at 7,000 RPM ($J = 1.09$) show relatively constant lift curve slope reductions of 3.6%, 4.1%, and 3.3% for wings with aspect ratios of 2 ($D/b = 0.46$), 3 ($D/b = 0.33$), and 4 ($D/b = 0.23$), respectively. Again, as discussed in the prior section, negligible variation is observed in the C_{L_α} from the clean wing results for both propellers in the pusher configuration [Figs. 18(b) and 19(b)].

For the case of maximum lift, calculated $C_{L_{max}}$ values are presented as a function of aspect ratio in Figs. 20 and 21 for the GWS 5×4.3 and GWS 3×3 propellers, respectively. The propeller slipstream has a larger effect on wings of lower aspect ratio (larger D/b) with larger magnitude $C_{L_{max}}$ values obtained at lower aspect ratios (larger D/b). Percentage $C_{L_{max}}$ increase results from the clean wing case for the highest rotation rate (lowest advance ratio) tested for each propeller and configuration are tabulated in Table 3. For

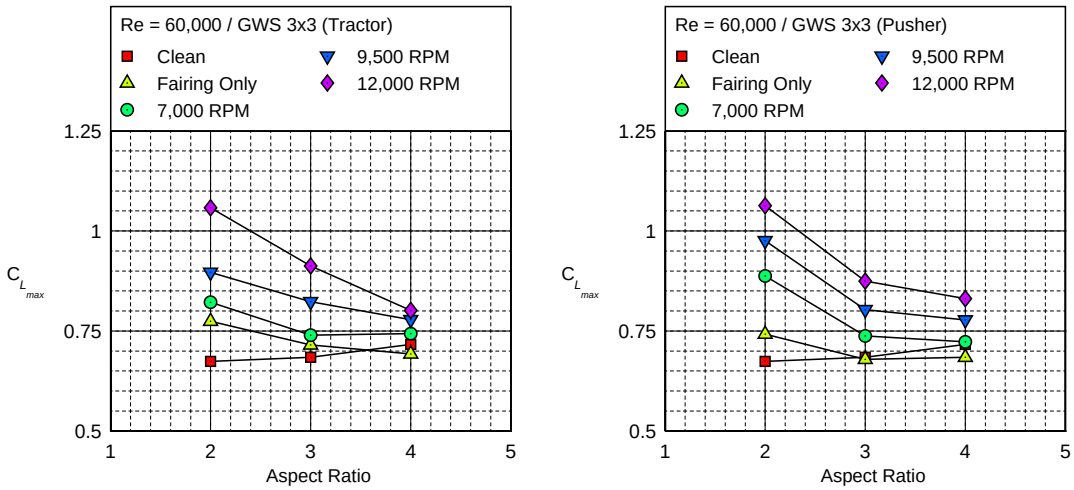

Figure 21. Effect of aspect ratio on the maximum lift, $C_{L_{max}}$, for rectangular flat-plate wings at a Reynolds number of 60,000 with the GWS 3×3 propeller in the (a) tractor and (b) pusher configuration.

Table 3. Percentage Increase in $C_{L_{max}}$ derived from Figs. 20 and 21

Configuration	Ω	J	$\mathcal{AR}$ (D/b)		
GWS 5×4.3			**2 (0.71)**	**3 (0.48)**	**4 (0.36)**
Tractor	8,000 RPM	0.6	46.0%	40.7%	19.6%
Pusher		0.61	43.7%	40.3%	30.2%
GWS 3×3			**2 (0.46)**	**3 (0.33)**	**4 (0.23)**
Tractor	12,000 RPM	0.64	56.9%	33.4%	11.8%
Pusher		0.63	57.6%	27.8%	15.9%

both propellers and configurations tested, $C_{L_{max}}$ increases as large at 57.6% are observed for the aspect ratio 2 wing. Both propeller results also showed a larger % $C_{L_{max}}$ increase in the pusher configurations results for the aspect ratio 4 flat-plate wings in comparison with the tractor configurations results. The results also show a clear relationship between the proportion of induced flow on the wing and the amount of maximum lift attained. Especially for wings with aspect ratios of 3 and 4, the degree of maximum lift and separation delay obtained is related to the propeller diameter-to-wingspan ratio (D/b). A larger D/b ratio and low J maximizes lift and separation delay for the wing.

2. Drag

The change in drag from the clean wing case (ΔC_D) of all three wings are coplotted as shown in Figs. 22 and 23 for the GWS 5×4.3 propeller in the tractor and pusher configurations at a Reynolds number of 60,000 and 80,000. The tractor configuration drag results exhibit variation in drag when a propeller at constant rotation rate operates at different flight velocities (34 ft/s and 45.3 ft/s). If the propeller operates closer to the windmill-brake state [Fig. 23(a)], reductions in drag are observed at angles of attack close to stall for the aspect ratio 2 and 3 wings. Less variation is observed for the pusher configuration cases close to the stall angle of attack. However, at high angles of attack, all wings and configurations showed higher drag in comparison with the clean wing case due to the propeller-induced flow effects.

An important observation from Figs. 22 and 23 is that in both the pusher and tractor configuration at low angles of attack (<9 deg), there is a consistent increase in drag for the aspect ratio 2 wing under propeller induced flow conditions from the clean wing state. The results give credence to conclusions found in Ref.

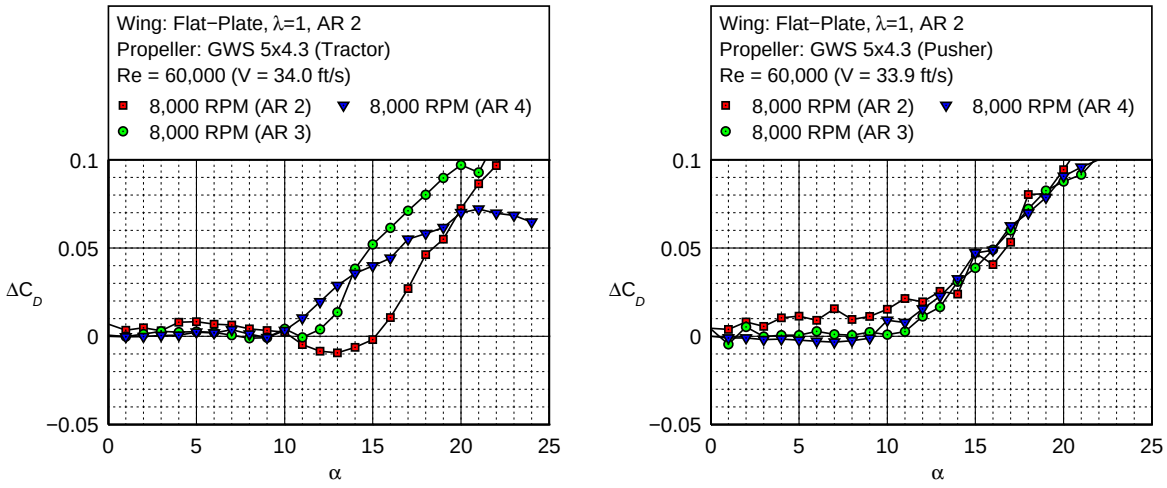

Figure 22. Change in C_D from clean wing case of different aspect ratio wings at a Reynolds number of 60,000 and the GWS 5×4.3 propeller at 8,000 RPM ($J = 0.60$) in the (a) tractor and (b) pusher configuration.

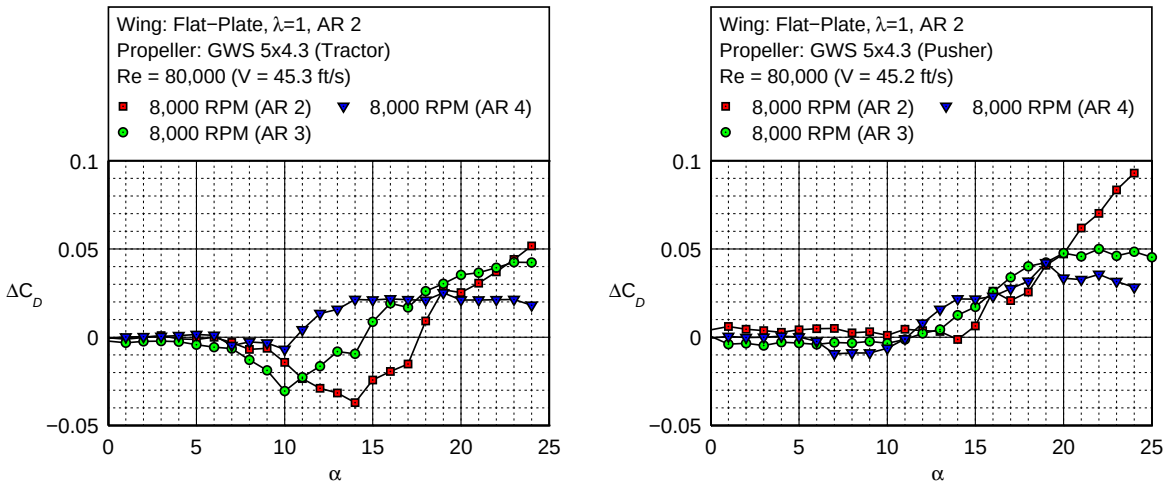

Figure 23. Change in C_D from clean wing case of different aspect ratio wings at a Reynolds number of 80,000 and the GWS 5×4.3 propeller at 8,000 RPM ($J = 0.81$) in the (a) tractor and (b) pusher configuration.

14, where tests performed on low aspect ratio wings exhibited an increase in drag at low Reynolds numbers due to the effect of propeller-induced flow. Finally, the drag results also show that the aspect ratio 2 and 3 wings are more affected by the propeller-induced flow especially in the tractor configuration.

V. Conclusions

Upon a review of literature, it was realized that there was an inconsistency associated with the results concerning the effects of propeller-induced flow on the aerodynamics of wings of different aspect ratios. To help address these discrepancies, wind tunnel experiments were performed on three flat-plate rectangular wings of aspect ratios 2, 3, and 4 using a custom designed low Reynolds number force balance (LRN-

FB) together with a setup that allowed different propeller-induced flow conditions to be set. Results of experiments performed for varying induced flow conditions showed significant aerodynamic performance differences due to varying propeller advance ratio (J) and wing aspect ratio [more importantly propeller diameter-to-wingspan ratio (D/b)].

Tractor configuration tests showed reductions in the lift curve slope when the propeller was operating close to or in the windmill-brake state. As a result, lift curve slope reductions from 3.6% to 13.4% were observed at high propeller advance ratios (windmill-brake state) for all wings and Reynolds numbers tested. A secondary relationship was also found between the lift curve slope and the propeller diameter-to-wingspan ratio (D/b) where higher lift curve slope reductions were observed at higher D/b ratios. It is important to note that as propeller rotation rate increased (decreasing advance ratio), the lift curve slope values increased for the tractor configuration. Similar reductions and variations of the lift curve slope under propeller induced flow were not, however, observed for the pusher configuration results.

In addition to lift curve slope effects, both configurations tested showed significant stall delay and maximum lift increasing effects due to the introduction of propeller-induced flow over the wing. Both effects were found to be closely related to both the propeller advance ratio and propeller diameter-to-wingspan ratio of the test cases. Maximum lift increases as large as 57.6% were observed for an aspect ratio 2 wing (low J, high D/b) with the GWS 3×3 propeller in the pusher configuration. The degree of stall delay and maximum lift increase obtained reduced as propeller advance ratio increased and propeller diameter-to-wingspan ratio decreased. In addition, higher maximum lift increases were observed for higher aspect ratio wings with propellers in the pusher configuration compared with the tractor configuration.

An increases in drag was found for both configurations (tractor and pusher) for all wings tested with increasing propeller rotation rate at high angles of attack. At low angles of attack, a consistent increase in drag for the aspect ratio 2 wing was observed for both configurations tested, whereas, similar magnitude increases in drag were not observed for the aspect ratio 3 and 4 cases. Finally, moments obtained due to variation of propeller rotation rate showed a delay in moment stall for the tractor configuration cases only. Both the tractor and pusher configuration cases though, showed increased magnitudes of moments in the post-stall conditions with decreasing propeller advance ratio (increasing rotation rate).

Acknowledgments

The authors thank Jeff Diebold and Matthew Dempsey for their assistance in wind tunnel testing. The authors would also like to thank Scott A. McDonald, Greggory L. Bennett, and David L. Switzer from the UIUC Electrical and Computer Engineering (ECE) machine shop for their guidance and support in machining the LRN-FB.

References

[1]Smelt, R. and Davies, H., "Estimation of Increase in Lift Due to Slipstream," ARC R&M 1788, 1937.

[2]Young, A. D. and Morris, D. E., "Note of Flight Tests on the Effect of Slipstream on Boundary Layer Flow," ARC R&M 1957, 1939.

[3]Young, A. D. and Morris, D. E., "Further Note of Flight Tests on the Effect of Slipstream on Boundary Layer Flow," RAE Rept. No. B.A. 1404b, 1939.

[4]Thompson, J. S., Smelt, R., Davison, B., and Smith, F., "Comparison of Pusher and Tractor Propeller Mounted on a Wing," ARC R&M 2516, 1940.

[5]Kuhn, R. E. and Draper, J. W., "Investigation of the Aerodynamic Characteristics of a Model Wing-Propeller Combination and of the Wing and Propeller Separately at Angles of Attack up to 90 deg," NACA 1263, 1956.

[6]Brenkmann, M., "Experimental Investigation of the Aerodynamics of a Wing in a Slipstream," UTIA 11, Toronto, ON, Canada, April 1957.

[7]Ribner, H. S., "Theory of Wings in Slipstreams," UTIA 60, Toronto, ON, Canada, May 1959.

[8]Witkowski, D. P., Johnston, R. T., and Sullivan, J. P., "Propeller/Wing Interaction," AIAA Paper 1989-0535, Reno, NV, 1989.

[9]Witkowski, D. P., Lee, A. K. H., and Sullivan, J. P., "Aerodynamic Interaction between Propellers and Wings," *Journal of Aircraft*, Vol. 26, No. 9, 1989, pp. 829–836.

[10]Catalano, F. M., "On the Effect of an Isolated Propeller Slipstream on Wing Aerodynamic Characteristics," *Acta Polytechnica*, Vol. 44, No. 3, 2004, pp. 8–14.

[11]Veldhuis, L. L. M., "Review of Propeller-Wing Aerodynamic Interference," *24th International Congress of the Aeronautical Sciences*, Yokohama, Japan, 2004.

[12]Veldhius, L. L. M., *Propeller-Wing Aerodynamic Interference*, Ph.D. thesis, Dept. of Aerospace Engineering, Delft University of Technology, Delft, The Netherlands, June 2005.

[13]Ananda, G. K., Deters, R. W., and Selig, M. S., "Propeller Induced Flow Effects on Wings at Low Reynolds Numbers." AIAA Paper 2013-3193, San Diego, CA, June 2013.

[14]Null, W., Noseck, A., and Shkarayev, S., "Effects of Propulsive-Induced Flow on the Aerodynamics of Micro Air Vehicles," AIAA Paper 2005-4616, Toronto, Ontario, June 2005.

[15]Shkarayev, S., Moschetta, J.-M., and Bataille, B., "Aerodynamic Design of Micro Air Vehicles for Vertical Flight," *Journal of Aircraft*, Vol. 45, No. 5, Sept.–Oct. 2008, pp. 1715–1724.

[16]Randall, R., Hoffmann, C.-A., and Shkarayev, S., "Longitudinal Aerodynamics of a Vertical Takeoff and Landing Micro Air Vehicle," *Journal of Aircraft*, Vol. 48, No. 1, Jan.–Feb. 2011, pp. 166–176.

[17]Randall, R., Wilson, L., and Shkarayev, S., "Flow Interactions around a Rapidly-Pitching MAV Wing," AIAA Paper 2012-0667, Nashville, TN, Jan. 2012.

[18]Sudhakar, S., Kumar, C., Arivoli, D., Dodamani, R., and Venkatakrishnan, L., "Experimental Studies of Propeller Induced Flow over a Typical Micro Air Vehicle," AIAA Paper 2013-0060, Grapevine, TX, Jan. 2013.

[19]Selig, M. S. and McGranahan, B. D., *Wind Tunnel Aerodynamic Tests of Six Airfoils for Use on Small Wind Turbines*, National Renewable Energy Laboratory, NREL/SR-500-35515, Golden, CO, 2004.

[20]Ananda, G. K., *Aerodynamic Performance of Low-to-Moderate Aspect Ratio Wings at Low Reynolds numbers*, Master's thesis, University of Illinois at Urbana-Champaign, Department of Aerospace Engineering, Urbana, IL, 2012.

[21]Ananda, G. K., Sukumar, P. P., and Selig, M. S., "Low-to-Moderate Aspect Ratio Wings Tested at Low Reynolds Numbers." AIAA Paper 2012-3026, New Orleans, LA, June 2012.

[22]Barlow, J. B., Rae Jr., W. H., and Pope, A., *Low-Speed Wind Tunnel Testing, Third Ed.*, John Wiley and Sons, New York, 1999.

[23]Kline, S. and McClintock, F. A., "Describing Uncertainty in Single-Sample Experiments," *Mechanical Engineering*, Vol. 75, 1953, pp. 3–8.

[24]Coleman, H. W. and Steele, Jr., W. G., *Experimentation and Uncertainty Analysis for Engineers*, John Wiley and Sons, New York, 1989.

[25]Deters, R. W. and Selig, M. S., "Static Testing of Micro Propellers," AIAA Paper 2008-6246, Honolulu, HI, Jan. 2008.

[26]Deters, R. W., *Performance and Slipstream Characteristics of Small-Scale Propellers at Low Reynolds Numbers*, Ph.D. thesis, Dept. of Aerospace Engineering, University of Illinois at Urbana-Champaign, Urbana, IL, Jan. 2014.

[27]Brandt, J. B., *Small-Scale Propeller Performance at Low Speeds*, Master's thesis, University of Illinois at Urbana-Champaign, Department of Aerospace Engineering, Urbana, IL, 2005.

[28]McCormick, B. W., *Aerodynamics, Aeronautics, and Flight Mechanics*, John Wiley & Sons, New York, NY, 2nd ed., 1995.